Modelling the mechanisms of quantum logic using the method of superimposed Fourier holograms based on the nonlinearity of the exposure characteristics of holographic recording media

A.V. Pavlov, V.V. Orlov

Abstract. **A Fourier-holography scheme with superimposed holograms and phase conjugation is considered. It is shown that the sub-holograms, arising from the recording of superimposed holograms due to quadratic nonlinearity of the exposure characteristics of holographic recording media, form the connections necessary for the realisation of the quantum-logic mechanism of sequential projection of the input vector onto the subspaces of the recorded images. A classical mechanism of the 'Linda' cognitive phenomenon belonging to the category of quantum-like ones is described. An experimental illustration of the self-sustained formation of sub-holograms due to the nonlinearity of the exposure characteristics of holographic recording media is given.**

1. Introduction

The method of superimposed holograms, i.e. holograms sequentially recorded on one section of the recording medium, is widely used in the development of content-addressable memory [1–3], in information processing systems [4–9], and in sensory and measuring systems [10–15]. One of the architectures often used to construct auto-associative memory (AAM) and information processing systems is the 4*f*-scheme of Fourier holography with phase conjugation [16, 17]. This scheme is often regarded as a realisation of the biologically motivated Hopfield AAM model; however, it also allows implementation of more complex models, for example, a linear predictor of random processes [18].

The properties of a holographic system and a model being implemented depend on the exposure characteristics of holographic recording media (EC HRM) used to record the superimposed holograms and in the phase-conjugate devices. For holographic AAM, of fundamental importance is the phase-conjugate nonlinearity originally included into the model and providing the 'cleanup' of the restored image from noise and distortion [16, 17]. At the same time, the EC HRM nonlinearity has only been analysed from the viewpoint of certain properties: signal-to-noise ratio [19, 20], sensitivity to distortions [21–24], additional diffraction orders [25], etc.

A.V. Pavlov, V.V. Orlov ITMO University, Kronverkskiy prosp. 49, 197101 St. Petersburg, Russia; e-mail: pavlov@phoi.ifmo.ru

Currently, attention is being attracted to biological, physical, and socially-motivated models of information processing, which, despite the difference in the nature of underlying processes, can be combined by the concept of 'network'. The network character is determined by the key role of interdependence and interaction of the elements uniting them into the ensembles possessing internal correlation as the most important attribute of information. From this standpoint, network methods undoubtedly comprise laser and coherent optics [26, 27], including holography [4–9, 28–31].

In recent years, the mathematical apparatus of quantum physics, namely, quantum logic [32] and quantum probability [33], has been increasingly used to describe a number of phenomena and processes previously considered as classical [26–31, 34–41]. The reason is that the problem of the inadequacy of their description by classical methods [41], for example, by means of the classical Kolmogorov probability theory [42], was successfully solved using quantum logic and quantum probability [34–40].

The global pendency of the interpretation problem in quantum physics [43, 44] in this case leaves room for a wide range of opinions on the fundamental causes and mechanisms stipulating the existence of analogies at the level of mathematical description of quantum mechanics and network processes [45]. It is important to note here that in some cases only those quantum physics tools are used which do not have a purely quantum specificity. For example, the property of noncommutativity as an attribute of quantum logic [32] and probability [33] made it possible to describe a number of experimentally observed phenomena [37, 38, 41], but it does not yet possess any exclusively quantum nature. Therefore, proceeding from the principle of minimising the explanation complexity, it is in our opinion advisable, without denying in principle the possibility of the presence of quantum mechanisms in network processes, to try to find out the classical mechanisms of such phenomena.

In this work, using the analysis of a Fourier-holography scheme with superimposed holograms and phase conjugation, it is shown, that the noncommutativity of logical-algebraic description operators can be caused by the nonlinearity of exposure characteristics of holographic recording media. Given the interdisciplinary aspect, the work is structured as follows. As a vivid example, Section 2 briefly describes the 'Linda' cognitive phenomenon [41] and its formal quantum-logical mechanism [37, 38]; then this mechanism is presented in the form of a network model. In Sections 3 and 4, modelling with the use of the method of superimposed Fourier holograms is considered. In Section 5, experimental confirmation of the formation of lattices with difference frequencies as a result of the EC HRM nonlinearity is presented. We have

adopted the terminology traditional for optics: ensembles and also the wave fields and images representing those ensembles in corresponding planes are considered according to the Huygens–Fresnel principle as a set of diffraction-limited point sources and are designated by the term 'image'.

2. The 'Linda' phenomenon and its network model

The description of the 'Linda' cognitive phenomenon and representation of its formal quantum-logical mechanism by the network model allows us to formulate a key question of its implementation in terms of the system properties and proceed to its solution.

The essence of the phenomenon [41] is as follows. A survey was conducted: respondents were briefly told about a fictional person named Linda and then offered to choose from a list of answers – what is Linda? Three answers were analysed: 'Feminist' (F), 'Teller' (T), and 'Feminist and Teller' ($F \& T$). The story was constructed in such a way as to evoke obvious associations with the answer 'Feminist' and none with 'Teller'. These two options in works [37, 38] were treated as incompatible, although in reality this is not so – they are independent. Based on the results of statistical processing of these responses, their probabilities were evaluated as $P(F) > P(F \& T) > P(T)$.

The experimental result $P(F \& T) > P(T)$ contradicts the classical probability theory for independent events [42], but is justified in quantum physics [33], which stimulated a quantum-logical description of its hypothetical mechanism [37, 38].

In accordance with [37, 38], we represent three images of 'Linda', 'Feminist' and 'Teller' by vectors L, F, and T, respectively. In quantum logic [32], operations are formalised by the projection operator, in our example – by projecting the system state vector L onto the subspaces $\mathcal{F}$ and $\mathcal{T}$ of the space of system states. Since the events F and T are independent, the vector L is sequentially projected onto $\mathcal{F}$ and $\mathcal{T}$, so that the result depends on the projection order as shown in Fig. 1 [37, 38]: if the vector L is at first projected onto the more probable subspace $\mathcal{F}$ and then the vector describing the state in $\mathcal{F}$ is projected onto $\mathcal{T}$, then the 'Teller' answer probability is higher than that in projecting L directly onto the subspace $\mathcal{T}$.
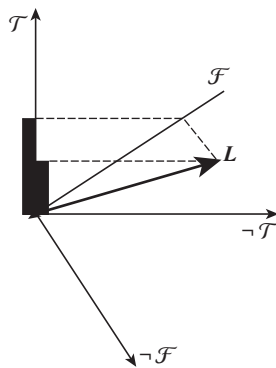
Figure 1. Principal scheme of conjunction applied to the 'Linda' phenomenon as a succession of projections of the state vector L onto the subspaces $\mathcal{F}$ and $\mathcal{T}$ represented for simplicity by the corresponding axes; the $\neg\mathcal{F}$ and $\neg\mathcal{T}$ axes represent negation defined in quantum logic as an orthogonal complement [34].

We represent the implementation of this mechanism in the form of a network model shown in Fig. 2. Each of the L, F, and T vectors describes the state of a certain image: L describes the current state of the system upon the perception of the information (story) about Linda, vectors F and T reflect the previously stored information on the respective images stored in the network connections (matrices of connection weights in the neural networks, holograms in optics, etc., described in subspaces $\mathcal{F}$ and $\mathcal{T}$). The independence of F and T means the lack of connection between these images in system training – each of them is independently recorded on its own hologram.
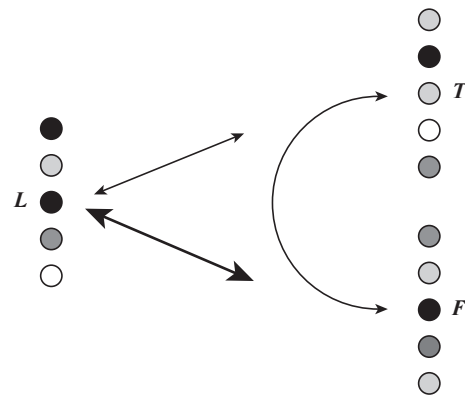
Figure 2. Network model of the 'Linda' phenomenon, the stage of conjunction: the line thickness between the images (ensembles) L, F and T correspond to the strength of associative connections arising upon submitting the image L to a system trained by reference images F and T; the arc represents a connection between F and T, required for the implementation of the model of successive projections and not explicitly specified in the training.

It is seen from Fig. 2 that, in order to implement sequential projecting of the state vector L onto the subspaces $\mathcal{F}$ and $\mathcal{T}$, first and foremost, a mechanism of self-sustained formation of the connection between F and T by the network is needed, as shown in Fig. 2 by the arc arrow. After that this connection should be used to project from $\mathcal{T}$ onto the subspace $\mathcal{F}$ a vector describing the result of projecting L onto $\mathcal{F}$. Below we show that the sought connection can be obtained by a known mechanism for the formation of combinational frequencies by a nonlinear system, which is also relevant in holography [25].

3. Holographic implementation

3.1. Recording of superimposed holograms

In quantum mechanics, the probability of an event B_{xy} (for example, finding a particle at a point with coordinates x, y), according to the Born rule, is given by the formula

$$P_{\psi}(B_{xy}) = \psi(x, y) \psi^{*}(x, y), \tag{1}$$

where ψ is the particle wave function or the probability amplitude [46]. Expression (1) formally corresponds to the classical definition of intensity in wave physics; the wave function $\psi(x, y)$ describes a field of complex amplitudes. This allows us

to use the field intensity $I(x,y) = \psi(x,y)\psi^*(x,y)$ as an analogue of the probability in a model of the phenomenon under study.

Consider the recording of two thin, i.e. possessing the property of angular invariance, superimposed Fourier holograms in a $4f$-scheme with spatial separation of off-axis point reference sources (Fig. 3). For simplicity, if possible, we will use the description of images as functions of only one variable x.
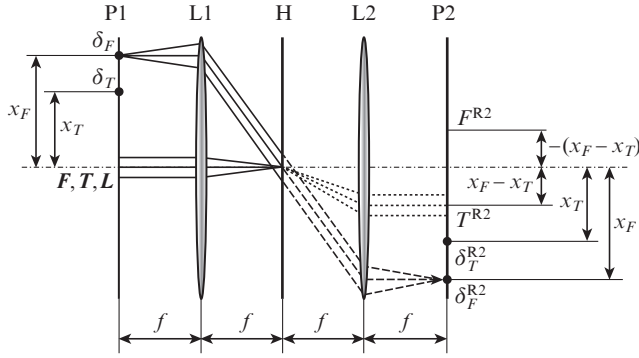

Figure 3. Scheme of $4f$ Fourier holography for two superimposed holograms: $\boldsymbol{F}, \boldsymbol{T}$ are the 'Feminist' and 'Teller' reference images; $\boldsymbol{L}$ is the 'Linda' image submitted to the recorded multiplex hologram; δ_F and δ_T are the off-axis point sources shifted by x_F and x_T relative to the main optical axis, respectively; P1 is the plane of images; L1, L2 are the first and second Fourier-transforming lenses with focal lengths f; H is the hologram plane (rear focal plane of the lens L1); P2 is the rear focal plane of the lens L2 (the plane of hologram responses). Dashed lines show the path of rays diffracting on the superimposed 'Feminist' hologram and restoring the image of the reference source δ_F^{R2} in the P2 plane; dotted lines show the path of rays diffracting on the sub-hologram resulting from quadratic nonlinearity and restoring the 'Teller' image $T^{R2}(x)$. The path of rays for the superimposed 'Teller' hologram restoring the image of the point source δ_T^{R2} is not shown.

When recording superimposed holograms in the Fourier plane (the rear focal plane of the first Fourier-transforming lens L1) in accordance with the scheme shown in Fig. 3, the intensity distributions to be recorded on the HRM are formed:

$$I_F(v) \propto [R_F\exp(\mathrm{j}\omega x_F) + \mathsf{F}(F(x))]$$
$$\times [R_F\exp(\mathrm{j}\omega x_F) + \mathsf{F}(F(x))]^*,$$
$$I_T(v) \propto [R_T\exp(\mathrm{j}\omega x_T) + \mathsf{F}(T(x))]$$
$$\times [R_T\exp(\mathrm{j}\omega x_T) + \mathsf{F}(T(x))]^*, \quad (2)$$

where $v = \zeta/\lambda f$ is the spatial frequency; ζ is the spatial coordinate in the Fourier plane H; $\omega = 2\pi v$ is the circular spatial frequency; R_F and R_T are the amplitudes of plane wave fronts, proportional to the amplitudes of the point reference sources described by the delta functions $\delta_F(x)$ and $\delta_T(x)$; x_F and x_T are their coordinates, respectively; and F is the Fourier-transform symbol.

We assume that nonlinear EC HRM can be represented by a power series, and we confine ourselves to the first two terms: linear and quadratic ones. If the formation of EC HRM nonlinearity occurs after the recording of all superimposed holograms, then the transfer function (for the amplitude HRM, the dependence of amplitude transmission on

spatial frequency) of the multiplex hologram $H(v) = H_F(v) + H_T(v)$ can be represented as follows:

$$H(v) = \eta_1\{[R_F\exp(\mathrm{j}\omega x_F) + \mathsf{F}(F(x))]$$
$$\times [R_F\exp(\mathrm{j}\omega x_F) + \mathsf{F}(F(x))]^*$$
$$+ [R_T\exp(\mathrm{j}\omega x_T) + \mathsf{F}(T(x))]$$
$$\times [R_T\exp(\mathrm{j}\omega x_T) + \mathsf{F}(T(x))]^*\}$$
$$+ \eta_2\{[R_F\exp(\mathrm{j}\omega x_F) + \mathsf{F}(F(x))]$$
$$\times [R_F\exp(\mathrm{j}\omega x_F) + \mathsf{F}(F(x))]^*$$
$$+ [R_T\exp(\mathrm{j}\omega x_T) + \mathsf{F}(T(x))]$$
$$\times [R_T\exp(\mathrm{j}\omega x_T) + \mathsf{F}(T(x))]^*\}^2, \quad (3)$$

where η_1 and η_2 are the coefficients of linear and quadratic terms of the expansion, depending on the HRM properties. Hereafter, the components (3) described by the linear term will be for brevity called a linear hologram (as a special case of the linear system). Now consider the quadratic term. Its decomposition (we omit cumbersome calculations) contains two terms describing the sought-for connection (shown by the arc in Fig. 2) between the reference sources $\delta_F(x)$ and $\delta_T(x)$ being not related in recording the hologram (3), and, in the presence of angular invariance, the reference images $F(x)$ and $T(x)$:

$$H_{FT}(v) = \eta_2[\mathsf{F}^*(F(x))\mathsf{F}(T(x))R_FR_T\exp(\mathrm{j}\omega(x_F - x_T))$$
$$+ \mathsf{F}(F(x))\mathsf{F}^*(T(x))R_FR_T\exp(-\mathrm{j}\omega(x_F - x_T))]. \quad (4)$$

Expression (4) describes a new hologram as part of the multiplex hologram (3), which emerges as a result of quadratic nonlinearity in EC HRM [25] (we call it a sub-hologram).

3.2. Multiplex hologram responses in direct light transmission

Upon presentation of the 'Linda' image $L(x)$ in the input image plane in the scheme shown in Fig. 3, the multiplex hologram (3) constructed within the +1-st diffraction orders described by the linear term (3) restores the images of point reference sources in the P2 plane (rear focal plane of the Fourier-transforming lens L2):

$$\delta_F^{R2}(\Delta) = \eta_1(L(x) \otimes F(x)), \quad (5a)$$
$$\delta_T^{R2}(\Delta) = \eta_1(L(x) \otimes T(x)), \quad (5b)$$

where the superscript R2 means reconstruction in the P2 plane; Δ is the coordinate in the P2 plane; and $\otimes$ is the symbol of correlation operation. Without loss of generality, we assume that the focal lengths of the lenses L1 and L2 are equal. Denote the amplitudes of the correlation functions at the points $\Delta = 0$ as scalar products $\langle\,\rangle$:

$$\max[L(x) \otimes F(x)] = \langle L(x), F(x)\rangle, \quad (6a)$$
$$\max[L(x) \otimes T(x)] = \langle L(x), T(x)\rangle. \quad (6b)$$

We introduce the ratio of amplitudes, for which, according to the experimental conditions [41], we have the inequality

$$k = \frac{\langle L(x), F(x) \rangle}{\langle L(x), T(x) \rangle} > 1. \qquad (7)$$

The sub-hologram (4) also forms responses in the P2 plane:

$$T^{R2(4)}(\Delta) = \eta_2 \mathsf{F}[\mathsf{F}(L(x))\mathsf{F}^*(F(x))\mathsf{F}(T(x))$$

$$\times R_F R_T \exp(j\omega(x_F - x_T))] = \eta_2 R_F R_T$$

$$\times \{T(x) * [L(x) \otimes F(x)] * \delta(x_F - x_T)\}, \qquad (8a)$$

$$R^{R2(4)}(\Delta) = \eta_2 \mathsf{F}[\mathsf{F}(L(x))\mathsf{F}(F(x))\mathsf{F}^*(T(x))$$

$$\times R_F R_T \exp(-j\omega(x_F - x_T))] = \eta_2 R_F R_T$$

$$\times \{F(x) * [L(x) \otimes T(x)] * \delta(x_T - x_F)\}, \qquad (8b)$$

where * is the convolution operation symbol; the designation (4) at the symbol R2 indicates the description (formula number in the paper) of the sub-hologram producing that response, and the sequence of records of the reconstructed images in (8a) and (8b) corresponds to the sequence of terms in (4).

For greater clarity, we neglect the diffraction broadening of the reconstructed images (8a) and (8b). This assumption is justified because of the fundamentally nonlinear subsequent phase conjugation in the P2 plane [16, 17]. Then expressions (8) take the form

$$T^{R2(4)}(\Delta) = \eta_2 R_F R_T \langle L(x), F(x) \rangle \{T(x) * \delta(x_F - x_T)\}, \quad (9a)$$

$$F^{R2(4)}(\Delta) = \eta_2 R_F R_T \langle L(x), T(x) \rangle \{F(x) * \delta(x_T - x_F)\}. \quad (9b)$$

Given (7), we present (9a) as

$$T^{R2(4)}(\Delta) = k\eta_2 R_F R_T \langle L(x), T(x) \rangle \{T(x) * \delta(x_F - x_T)\},$$

whence we obtain the ratio of intensities of the reconstructed sub-hologram (4) in the P2 plane of the images (8a) and (8b) ('Teller'/'Feminist'):

$$V^{(4)} = \frac{\langle T^{R2(4)}(\Delta), T^{R2(4)}(\Delta) \rangle}{\langle F^{R2(4)}(\Delta), F^{R2(4)}(\Delta) \rangle} = k^2 \frac{\langle T(x), T(x) \rangle}{\langle F(x), F(x) \rangle}. \qquad (10)$$

3.3. Back-propagation image reconstruction (linear hologram)

Consider the fields formed in the P1 plane by a linear hologram on the main optical axis as a result of conjugation of the wavefronts in the plane P2 from the reconstructed images of point reference sources (5a) and (5b) (Fig. 4). We assume that there is no conjugation of the wavefront in the region of main optical axis in the P2 plane.

As before, we neglect the diffraction blurring of reconstructed images and consider the passage of radiation from the point source $\delta_F^{R2}(\Delta)$; for the point source $\delta_T^{R2}(\Delta)$ the analysis is similar. Linear hologram forms several diffraction orders in P1 (when choosing signs in pre-exponential expressions, the
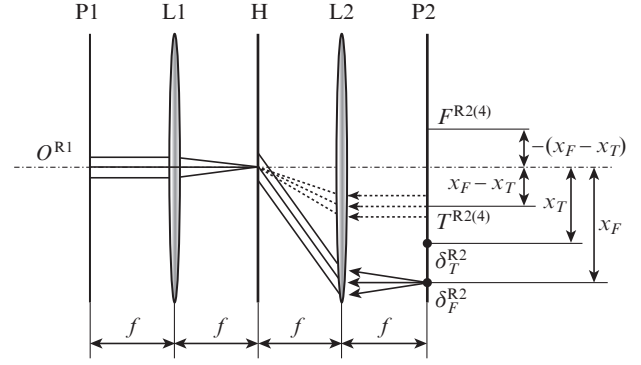

Figure 4. Scheme of 4f Fourier holography for two superimposed holograms at the stage of phase conjugation in the P2 plane: $F^{R2(4)}$ and $T^{R2(4)}$ are the 'Feminist' and 'Teller' images reconstructed by sub-hologram (4); δ_F^{R2} and δ_T^{R2} are the point sources formed by the phase-conjugate device (not shown in the diagram). The other symbols are the same as in Fig. 3.

coordinate inversion in the P2 plane due to the nonrealisability of the inverse Fourier transform hase been taken into account):

$$\eta_1 \mathsf{F}[(R_F^{R2} \exp(j\omega x_F))\{[R_F \exp(j\omega x_F) + \mathsf{F}(F(x))]$$

$$\times [R_F \exp(j\omega x_F) + \mathsf{F}(F(x))]^* + [R_T \exp(j\omega x_T)$$

$$+ \mathsf{F}(T(x))][R_T \exp(j\omega x_T) + \mathsf{F}(T(x))]^*\}] =$$

$$= \eta_1 \mathsf{F}[R_F^{R2} R_F R_F \exp(j\omega x_F) + R_F^{R2} R_F \mathsf{F}^*(F(x))$$

$$\times \exp(2j\omega x_F) + R_F^{R2} R_F \mathsf{F}(F(x)) + R_F^{R2} \mathsf{F}(F(x))$$

$$\times \mathsf{F}^*(F(x)) \exp(j\omega x_F) + R_F^{R2} R_T R_T \exp(j\omega x_F)$$

$$+ R_F^{R2} R_T \mathsf{F}^*(T(x)) \exp(j\omega(x_T + x_F)) + R_F^{R2} R_T$$

$$\times \mathsf{F}(T(x)) \exp(j\omega(x_F - x_T)) + R_F^{R2} \mathsf{F}(T(x))$$

$$\times \mathsf{F}^*(T(x)) \exp(j\omega x_F)]. \qquad (11)$$

The traditional holographic AAM [16, 17] uses the third term in (11) describing the field in the main optical axis region – the reconstructed reference

$$F^{R1(11.3)}(x) = \eta_1 R_F \delta_F^{R2} * F(x) = \eta_1 R_F F(x) \langle L(x), F(x) \rangle$$

$$= \eta_1 k R_F F(x) \langle L(x), T(x) \rangle, \qquad (12a)$$

where the superscript (11.3) means that the described field is formed by the third term in expression (11), while δ^{R2} (without coordinate) is the real amplitude of the point source corresponding to the lower symbol, and (7) is taken into account. Similarly, for the source $\delta_T^{R2}(\Delta)$ in the same region around the main optical axis, we have

$$T^{R1(11.3)}(x) = \eta_1 R_T \delta_T^{R2} * T(x) = \eta_1 R_T T(x) \langle L(x), T(x) \rangle$$

$$= \eta_1 R_T T(x) \langle L(x), T(x) \rangle. \qquad (12b)$$

Expressions (12a) and (12b) describe the operation of holographic AAM [16, 17]. The intensity ratio of the recon-

structed 'Teller'/'Feminist' images, superimposed on each other in the region of main optical axis [using the same order as in (10)], takes the form

$$V^{(11.3)} = \left(\frac{\langle T^{R1(11.3)}(x)\, T^{R1(11.3)}(x)\rangle}{\langle F^{R1(11.3)}(x)\, F^{R1(11.3)}(x)\rangle}\right)^2$$

$$= \frac{\langle T(x), T(x)\rangle}{\langle F(x), F(x)\rangle}\left(\frac{\langle L(x, T(x))\rangle}{\langle L(x), F(x)\rangle}\right)^2 = \frac{1}{k^2}\frac{\langle T(x), T(x)\rangle}{\langle F(x), F(x)\rangle}. \quad (13)$$

The reconstructed image $T^{R1(11.3)}(x)$ is weakened correlated to the image $F^{R1(11.3)}(x)$ that exactly reflects the conditions for the formation of the 'Linda' image in the experiment [41]. In arranging the iterative procedure at the expense of phase conjugation in the P1 plane, only the 'Feminist' image (12a) will finally remain from the sum of images (12a) and (12b), while the 'Teller' image (12b) will be suppressed – thus we come to the classic AAM model [16, 17].

3.4. Back-propagation image reconstruction (quadratic sub-hologram)

Consider the result of diffraction on the sub-hologram (4) of conjugate wavefronts from images (9a) and (9b). For image (9a), the distribution of amplitudes in the plane P1 appears as

$$T^{R1(14)}(x) = F\{\eta_2 F(T^{R2(4)}(x))\exp(j\omega(x_F - x_T))$$

$$\times [F^*(F(x))F(T(x))R_F R_T \exp(j\omega(x_F - x_T))$$

$$+ F(F(x))F^*(T(x))R_F R_T \exp(-j\omega(x_F - x_T))]\}. \quad (14)$$

Hereinafter, using the previously accepted assumption on the equality of the focal lengths L1 and L2, and taking into account the coordinate inversion, we replace the coordinate Δ in the P2 plane by x. We have three orders of diffraction:

1) zero diffraction order on the sub-hologram (4) is localised in the P1 plane within a region centred at the coordinate $(x_F - x_T)$;

2) +1-st diffraction order is localised within a region centred on the main optical axis, i.e. superimposed onto the images $F^{R1(11.3)}(x)$ (12a) and $T^{R1(11.3)}(x)$ (12b):

$$T^{R1(14.2)}(x) = F[\eta_2 F(T^{R2(4)}(x))F(F(x))F^*(T(x))R_F R_T]$$

$$= \eta_2 R_F R_T T^{R2(4)}(x) * (F(x) \otimes T(x)); \quad (15a)$$

3) −1-st order is localised within a region centred at the coordinate $2(x_F - x_T)$:

$$T^{R1(14.1)}(x) = F[\eta_2 F(T^{R2(4)}(x))\exp(j\omega 2(x_F - x_T))$$

$$\times F^*(F(x))F(T(x))R_F R_T] = \eta_2 R_F R_T T^{R2(4)}$$

$$\times (x + 2(x_F - x_T)) * (T(x) \otimes F(x)).$$

A similar situation also takes place in diffraction of the source $F^{R2(4)}(x)$ on the sub-hologram (4): in the region centred at the coordinate $-(x_F - x_T)$ we obtain the image $F^{R2(4)}(x)$ that passes without diffraction and coincides with the image $F^{R1(11.7)}(x)$ reconstructed by the linear part of hologram (3), and also the first two diffraction orders: +1-st order centred on the main optical axis and −1-st order located at a distance $-2(x_F - x_T)$ from it. We are interested in the +1-st order:

$$F^{R1(14.1)}(x) = F[\eta_2 F(F^{R2(4)}(x))F(F^*(x))F(T(x))R_F R_T]$$

$$= \eta_2 R_F R_T F^{R2(4)}(x) * (T(x) \otimes F(x)). \quad (15b)$$

In the case of correct phase conjugation, all images are real; the resulting image in the region centred on the main optical axis takes the form

$$O^{R1}(x) = F^{R1}(x) + T^{R1}(x), \quad (16)$$

where

$$F^{R1}(x) = F^{R1(11.3)}(x) + F^{R1(14.1)}(x),$$

$$T^{R1}(x) = T^{R1(11.3)}(x) + T^{R1(14.2)}(x).$$

To estimate the ratio of intensities, we neglect the blurring of images $T^{R1(14.2)}(x)$ and $F^{R1(14.1)}(x)$ as a result of their convolution with cross-correlation functions $[T(x) \otimes F(x)]$, and replace the latter with scalar products.

Then we have

$$F^{R1}(x) = \eta_1 k R_F F(x)\langle L(x), T(x)\rangle + \eta_2 F^{R2(4)}(x)$$

$$* (T(x) \otimes F(x)) = \eta_1 k R_F F(x)\langle L(x), T(x)\rangle$$

$$+ \eta_2^2 R_F^2 R_T^2 \langle L(x), T(x)\rangle F(x)\langle T(x), F(x)\rangle$$

$$= F(x)\langle L(x), T(x)\rangle[k\eta_1 R_F + \eta_2^2 R_F^2 R_T^2 \langle T(x), F(x)\rangle],$$

$$T^{R1}(x) = \eta_1 \langle L(x), T(x)\rangle R_T T(x) + \eta_2 T^{R2(4)}(x)$$

$$* (F(x) \otimes T(x)) = \eta_1 \langle L(x), T(x)\rangle R_T T(x)$$

$$+ \eta_2^2 [R_F^2 R_T^2 \langle L(x), T(x)\rangle T(x)] * (T(x) \otimes F(x))$$

$$= T(x)\langle L(x), T(x)\rangle[\eta_1 R_T + k\eta_2^2 R_F^2 R_T^2 \langle T(x), F(x)\rangle].$$

Hence, the ratio of intensities in the resulting image is

$$V^{R1} = \frac{\langle T(x), T(x)\rangle}{\langle F(x), F(x)\rangle}\left(\frac{\eta_1 R_T + k\eta_2^2 R_F^2 R_T^2 \langle T(x), F(x)\rangle}{k\eta_1 R_F + \eta_2^2 R_F^2 R_T^2 \langle T(x), F(x)\rangle}\right)^2.$$

We introduce the ratio $r_\eta = \eta_2^2/\eta_1$ of diffraction efficiencies of the linear and quadratic holograms in the composition of the multiplex hologram (3), and, for greater clarity, we adopt the assumption on the equality of amplitudes of the reference beams in recording the superimposed holograms. Then,

$$V^{R1} = \frac{\langle T(x), T(x)\rangle}{\langle F(x), F(x)\rangle}\left(\frac{1 + kr_\eta R_F^2 R_T \langle T(x), F(x)\rangle}{k + r_\eta R_T^2 R_F \langle T(x), F(x)\rangle}\right)^2.$$

We are interested in a change in the balance of intensities 'Teller' and 'Feminist' in the resultant image due to the action of the sub-hologram (4) with respect to their balance provided by the linear multiplex hologram, i.e. in the ratio

$$V = \frac{V^{R1}}{V^{(11.3)}} = \left(k\frac{1 + kr_\eta R_F^2 R_T \langle T(x), F(x)\rangle}{k + r_\eta R_T^2 R_F \langle T(x), F(x)\rangle}\right)^2$$

$$= \left(\frac{1 + kr_\eta R_F^2 R_T \langle T(x), F(x)\rangle}{1 + \frac{1}{k}r_\eta R_T^2 R_F \langle T(x), F(x)\rangle}\right)^2. \quad (17)$$

It is easy to see that, since $k > 1$ in accordance with experimental conditions [41], $V > 1$ and increases with increasing k.

We should note that the conjugation of wavefronts in the P2 plane was only considered above with regard to four images (5a), (5b), (9a), and (9b) localised outside the main optical axis. The field on the main optical axis in the P2 plane (zero diffraction order on the hologram with direct passage of light) is not subject to conjugation with the aim of interference elimination.

4. Discussion

Thus, the sought-for connection between the images $F(x)$ and $T(x)$ in recording their superimposed holograms, indicated by the arc in Fig. 2, can be obtained at the expense of the EC HRM quadratic nonlinearity providing the self-sustained formation of the sub-hologram (4). The mechanism of successive projections is realised by the phase conjugation in the plane of hologram responses.

The result $P(F\&T) > P(T)$ being observed in the experiment [41] and contradicting the classical probability theory is due to a sigmoid EC of the sensor recording the resultant image (16). We obtain the intensity ratio (13) in linear recording of the superimposed holograms, – the coefficient k is fairly large under the conditions of the experiment, and when the sensor is optimised with respect to intensity difference in the brighter 'Feminist' image, the 'Teller'' image falls into the deadband and is not recorded. If the sensor sensitivity is optimised with respect to the 'Teller' image, the 'Feminist' image falls into the saturation range and is not recorded.

According to (17), the action of quadratic sub-hologram (4) 'pulls' the 'Teller' image into the operating range. As a result, both 'Feminist' and 'Teller' images are recorded, i.e. we have $P(F\&T)$. Herewith, it follows from expression (17) that the greater the initial difference in the amplitudes of images (i.e., the larger the k), the more efficient the operation of the quadratic sub-hologram (4).

Thus, to obtain the discussed quantum-like phenomenon, the nonlinearities both of the EC HRM for recording the superimposed holograms and the sensor recording the image reconstructed by the holographic scheme are of importance.

5. Experimental part

The purpose of experimental illustration at this stage is to demonstrate the presence and operation of the sub-hologram (4) autonomously formed in the recording of superimposed holograms due to quadratic nonlinearity of the EC HRM. We used a PFG-03m HRM ('Slavich' Scientific Production Association) processed with bleaching at a photo-layer thickness of ~ 7 μm and a recording wavelength of 633 nm. The superimposed holograms are recorded with a planar signal wave incident onto the plate along the normal (along the main optical axis in Fig. 3). Plane reference waves are directed at an angle of $33.3°$ to the reference wave (the main optical axis in Fig. 3) when recording the first superimposed hologram, and at an angle of $36.3°$ when recording the second one.

Figure 5 shows the multiplex hologram responses experimentally obtained in illumination by a signal wave. The diffraction efficiency was 27% and 18% for the first diffraction orders corresponding to the linear terms in expression (3) and representing the reconstructed reference waves used to record the superimposed holograms, and 8% and 2.9% for the responses formed by the sub-hologram (4). Different diffraction

Figure 5. Multiplex hologram responses: 1 is the zero diffraction order; 2, 3 are the 1st diffraction orders; 4, 5 are the responses due to diffraction on the lattice having a difference frequency and resulting from the EC HRM nonlinearity.

efficiencies for the responses of the same orders are stipulated by different deviations from the Bragg condition: for a linear hologram, the illumination conditions coincided with the recording conditions, i.e., the Bragg condition was fulfilled, while for the sub-hologram these conditions were significantly different.

6. Conclusions

Thus, the mechanism typical of quantum logic and consisting in sequential projecting of the input vector onto the subspaces in which logical rules (references) are stored can be implemented by the classical method of superimposed Fourier holograms with phase conjugation due to quadratic nonlinearity of the exposure characteristics of holographic recording media.

Information in network systems is stored in the form of a structure of connections of their elements, which always has a material carrier (in particular, for cognitive systems, this is a structure of inter-neuronal connections). Therefore, the result presented here gives a reason to believe that a number of network phenomena treated as the quantum-like ones [34–40], in particular, the 'Linda' cognitive phenomenon [41], may be based on the classical mechanism due to the nonlinearity of material carriers of network connections.

We note that this conclusion correlates with the results of work [47] and a series of works [48–50]. In work [47], it is shown that the Fourier holographic scheme generates the algebra of fuzzy-valued logic: the hologram stores the reference as a rule of logical inference, while the Fourier hologram response is described as the 'Generalised Modus Ponens' logical inference. At the same time, it is shown in the series of works [48–50] that any measurement in both quantum mechanical and classical systems can be represented as a form of the 'Generalised Modus Ponens' logical inference, i.e. an inference in the class of fuzzy-valued logics. Herewith, the algebra of fuzzy-valued logics does not address the possible quantum nature of the described phenomena and mechanisms.

To sum it up, we should particularly emphasise that the conclusion about the classical mechanism of quantum-like logic generation (in particular, the noncommutativity of logical operators) in the Fourier holography scheme with phase conjugation and nonlinear recording of superimposed holograms as a special case of network systems should not be treated as a denial of the possibility of the existence of quantum effects or quantum nature of the processes under consideration, stipulating these effects, but only as an attempt of a simple and minimally sufficient explanation in the frame of the known classical approaches.

References

1. Betin A.Yu., Bobrinev V.I., Evtikhiev N.N., Zherdev A.Yu., Zlokazov E.Yu., Lushnikov D.S., Markin V.V., Odinokov S.B., Starikov S.N., Starikov R.S. *Quantum Electron.*, **43**, 87 (2013) [*Kvantovaya Elektron.*, **43**, 87 (2013)].
2. Betin A.Yu., Bobrinev V.I., Odinokov S.B., Evtikhiev N.N., Starikov R.S., Starikov S.N., Zlokazov E.Yu. *Appl. Opt.*, **52**, 8142 (2013).
3. Betin A.Yu., Bobrinev V.I., Verenikina N.M., Donchenko S.S., Evtikhiev N.N., Zlokazov E.Yu., Odinokov S.B., Starikov S.N., Starikov R.S. *Quantum Electron.*, **45**, 771 (2015) [*Kvantovaya Elektron.*, **45**, 771 (2015)].
4. Longuet-Higgins H.C. *Nature*, **217**, 104 (1968).
5. Gabor D. *Nature*, **217**, 584 (1968).
6. Mager H.J., Wess O., Waidelich W. *Opt. Commun.*, **9**, 156 (1973).
7. Foster D.J., Wilson M.A. *Nature*, **440**, 680 (2006).
8. Pavlov A.V. *Quantum Electron.*, **46**, 759 (2016) [*Kvantovaya Elektron.*, **46**, 759 (2016)].
9. Pavlov A.V. *Quantum Electron.*, **47**, 335 (2017) [*Kvantovaya Elektron.*, **47**, 335 (2017)].
10. Borkova V.N., Zubov V.A., Kraiskiy A.V. *Opt. Spektrosk.*, **63**, 384 (1987).
11. Kraiskii A.V., Mironova T.V. *Quantum Electron.*, **45**, 759 (2015) [*Kvantovaya Elektron.*, **45**, 759 (2015)].
12. Lyavshuk I.A., Lyalikov A.M. *Quantum Electron.*, **36**, 154 (2006) [*Kvantovaya Elektron.*, **36**, 154 (2006)].
13. Granovskii V.A., Kudryavtsev M.D., Ryskin A.I., Shcheulin A.S. *Opt. Spektrosk.*, **106**, 855 (2009).
14. Angervaks A.E., Granovskii V.A., Kudryavtsev M.D., Ryskin A.I., Shcheulin A.S. *Opt. Spektrosk.*, **112**, 343 (2012).
15. Orlov V.V. *Quantum Electron.*, **47**, 773 (2017) [*Kvantovaya Elektron.*, **47**, 773 (2017)].
16. Soffer B.H., Dunning G.J., Owechko Y., Marom E. *Opt. Lett.*, **11**, 118 (1986).
17. Paek E.G., Psaltis D. *Opt. Eng.*, **26**, 428 (1987).
18. Pavlov A.V. *Opt. Spektrosk.*, **98**, 1033 (2005).
19. Shubnikov E.I. *Opt. Spektrosk.*, **62**, 450 (1987).
20. Shubnikov E.I. *Opt. Spektrosk.*, **62**, 653 (1987).
21. Kuleshov A.M., Shubnikov E.I. *Opt. Spektrosk.*, **55**, 161 (1983).
22. Kuleshov A.M., Pavlov A.V., Shubnikov E.I. *Opt. Spektrosk.*, **59**, 415 (1985).
23. Pavlov A.V. *Opt. Spektrosk.*, **70**, 1337 (1991).
24. Aleksandrina S.A., Kuleshov A.M. *Opt. Spektrosk.*, **68**, 652 (1990).
25. Orlov V.V. *Pis'ma Zh. Tekh. Fiz.*, **30** (24), 77 (2004).
26. Danilov O.B., Rozanov N.N., Solov'yov N.A., Soms L.N. *Opt. Spektrosk.*, **120**, 151 (2016).
27. Oraevskii A.N. *Quantum Electron.*, **30**, 457 (2000) [*Kvantovaya Elektron.*, **30**, 457 (2000)].
28. Peruš M., Bischof H., Caulfield H.J., Loo C.K. *Appl. Opt.*, **43**, 6134 (2004).
29. Loo C.K., Peruš M., Bischof H. *Opt. Spektrosk.*, **99**, 233 (2005).
30. Loo C.K., Peruš M., Bischof H. *Opt. Zh.*, **72**, 358 (2005).
31. Tay N.W., Loo C.K., Peruš M. *Cognitive Computation*, **2**, 297 (2010).
32. Birkhoff G., von Neumann J. *Ann Math.*, **37**, 823 (1936), https://doi.org/10.2307/1968621.
33. Holevo A.S. *Itogi Nauki Tekh. Ser. Sovr. Probl. Mat. Fundam. Napravl.*, **83**, 5 (1991).
34. Khrennikiv A. *Frontiers in Physics*, **3**, 77 (2015).
35. Asano M., Basieva I., Khrennikiv A., Ohya M., Tanaka Y., Yamato I. *Foundations of Physics*, **45**, 1362 (2015), DOI: 10.1007/s10701-015-9929-y.
36. Menskii M.B. *Usp. Fiz. Nauk.*, **170**, 631 (2000).
37. Busemeyer J.R., Pothos E., Franco R., Trueblood J.S. *Psychological Rev.*, **118**, 193 (2011).
38. Trueblood J.S., Pothos E.M., Busemeyer J.R. *Frontiers in Psychology*, **5**, 322 (2014).
39. Moreira C., Wichert A. *Front. Phys.*, **4**, 26 (2016), DOI: 10.3389/fphy.2016.00026.
40. Piotrowski E.W., Sładkowski J., in *The Palgrave Handbook of Quantum Models in Social Science* (London: Palgrave Macmillan, 2017) p. 39.
41. Tversky A., Kahneman D. *Psychological Rev.*, **90**, 293 (1983).
42. Kolmogorov A.N. *Foundations of Probability* (New York: Chelsea Publishing Company, 1950; Moscow: Nauka, 1974).
43. Grib A.A. *Usp. Fiz. Nauk.*, **183**, 1337 (2013).
44. Lipkin A.I., Nakhmanson R.S., Pilan A.M., Panov A.D., Lesovik G.B., Tsekhmistro I.Z., Menskii M.B. *Usp. Fiz. Nauk.*, **171**, 437 (2001).
45. Meijer D.K.F., Raggett S., in *Quantum Mind Extended, 2014b*; https://quantum-mind.co.uk/wp-content/uploads/2014/11/Quantum-Ph-rev-def-2.pdf.
46. Feynman R., Leighton R., Sands M. *The Feynman Lectures on Physics* (Palo Alto and London: Addison Wesley Pub. Com., 1964).
47. Pavlov A.V. *Opt. Spektrosk.*, **90**, 515 (2001).
48. Ishikawa S. *Fuzzy Sets and Systems*, **87**, 181 (1997).
49. Ishikawa S. *Fuzzy Sets and Systems*, **90**, 277 (1997).
50. Ishikawa S. *Fuzzy Sets and Systems*, **100**, 291 (1998).